

Differential settlements in foundations under embankment load: Theoretical model and experimental verification

Changdan Wang^{*1,2}, Shunhua Zhou¹, Binglong Wang¹, Peijun Guo² and Hui Su²

¹Key Laboratory of Road and Traffic Engineering of the Ministry of Education,
Tongji University, 4800 Cao'an Road, Shanghai, 201804 China
²Department of Civil Engineering, McMaster University,
1280 Main Street West, Hamilton, Ontario, L8S 4L6 Canada

(Received May 15, 2014, Revised November 10, 2014, Accepted November 17, 2014)

Abstract. To research and analyze the differential settlements of foundations specifically, site investigations of existing railways and metro were firstly carried out. Then, the centrifugal test was used to observe differential settlements in different position between foundations on the basis of investigation. The theoretical model was established according to the stress diffusion method and Fourier method to establish an analytical solution of embankment differential settlement between different foundations. Finally, theoretical values and experimental values were analyzed comparatively. The research results show that both in horizontal and vertical directions, evident differential settlement exists in a limited area on both sides of the vertical interface between different foundations. The foundation with larger elastic modulus can transfer more additional stress and cause relatively less settlement. Differential settlement value decreases as the distance to vertical interface decreases. In the vertical direction of foundation, mass differential settlement also exists on both sides of the vertical interface and foundation with larger elastic modulus can transfer more additional stress. With the increase of relative modulus of different foundations, foundation with lower elastic modulus has larger settlement. Meanwhile, differential settlement is more obvious. The main error sources in theoretical and experimental values include: (a) different load form; (b) foundation characteristics differences; (c) modulus conversion; (d) effect of soil internal friction.

Keywords: railways embankment; vertical interface; differential settlement; existing railways investigation; theoretical model; centrifugal test

1. Introduction

The high-speed railways that are quick, safe, efficient and comfortable way of transportation have become a common trend of transportation in many countries. However, large settlement of infrastructure may severely endanger the life of passengers in high-speed railways. Therefore, proper control of the foundation settlement is very important for the safe operation of high-speed railways. There is no way to replace the embankments with bridges, in most instances, due to the strict settlement control standards, as shown in Table 1 (Ministry of Railways of People's Republic of China 2009). The method to replace the embankments with bridges are forced, and be

*Corresponding author, Associate Research, E-mail: 2008wangchangdan@tongji.edu.cn

Table 1 Embankment settlement control standards in post-construction stage of ballasted track high-speed railways in China

Design speed (km/h)	Embankment zone (cm)	Bridge-embankment transitional zone (cm)	Settlement rate (cm/year)	Slope ratio
250	10	5	3	1/1000
300, 350	5	3	2	1/1000

also more costly (Liu *et al.* 2007, Wang *et al.* 2013). The embankment of high-speed railways is required to have high strength, stiffness, excellent stability, and durability. The post-construction settlement of embankment, which is mainly affected by foundation, plays a significant role in the embankment design and safe operation of high-speed railways (Wang *et al.* 2014).

Controlling embankment post-construction settlement, especially differential settlement, has become a key issue for embankment engineering in high-speed railways. Moreover, how to calculate the foundation differential settlement accurately is one of the important issues for controlling settlement. The main reasons are summarized as the following: (1) the new theory and technology have not matured yet, and higher requirements are needed for the ability of professional personnel and measuring methods; (2) the theoretical aspect and construction methods need to be taken in account when estimating foundation settlement. From the viewpoint of practical applications, the method is expected to be simple and applicable to various engineering conditions with less and easily measured parameters; (3) various quantities, such as the applied load, stresses in soils and the stress history in soil, may affect the calculation of foundation settlement (Braja 2008, Puzrin *et al.* 2010, Wu and Yu 2006, Anderson *et al.* 2007, Matyas and Rothenburg 1996). In general, the foundation settlement analysis is complex and the results may not be reliable if any of these quantities is determined incorrectly.

The foundation settlement calculation methods can be divided into two categories: (1) Empirical coefficient correction method (ECCM) that is based on the foundation complexity with engineering practice that has lower computational accuracy; (2) Modified method from design mode and measure, which usually has relatively improved computational accuracy. The modified methods of settlement calculation mainly include: (a) settlement calculation method was improved by geological history of Soils; (b) the soil stress state is considered to improve the settlement calculation; (c) the soil settlement characteristics are used to improve settlement calculation; and (d) optimization of settlement calculation method and process (Toshihiro *et al.* 2005, Mylonakis and Gazetas 1998, Fenton and Griffiths 2002, Han and Gabr 2002, Mutsumi *et al.* 2011, Wang 2007, Shideh *et al.* 2010).

The technology to control the embankment differential settlement has made great development during the past decades. The research on embankment settlement mostly focuses on horizontally layered soils. There is only limited research on additional stress transfer and settlement of vertical bounding layer between different structures or foundations. In particular, researchers only have qualitative knowledge on mechanical mechanism of embankment differential settlement under static (or dynamic) load when foundation properties change suddenly along the embankment. In this paper, following an investigation on existing railways, a series of model tests are conducted to study differential settlement in different position and depth between foundations. Then a theoretical model is developed according to the stress diffusion method to explore an analytical solution of embankment differential settlement between different foundations with the Fourier

method. Finally, theoretical results are compared with experimental data. The proposed method and criteria for embankment differential settlement calculations can be used in different stage of railway engineering such as railway route selection, embankment design and construction, track structure selection and maintenance and so on.

2. Site investigation result analysis

The research is based on the investigation of differential settlements in railways in operation in China (including Beijing-Shanghai railway, Shanghai-Hangzhou railway, Datong-Qinhuangdao railway, Shanghai metro and Nanjing metro). Some investigation results are show in Figs. 1-2, while Table 2 presents a summary of the mechanisms. The deterioration of railway operation state caused by embankment differential settlement is widespread in soft soils, especially in the area between different foundations or structures. Moreover, such deterioration phenomenon is more

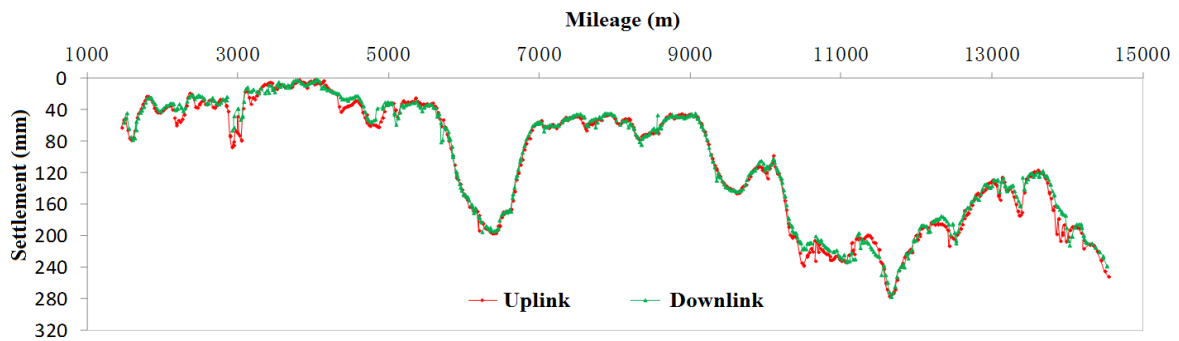


Fig. 1 Differential settlement of S-city Metro Line 1

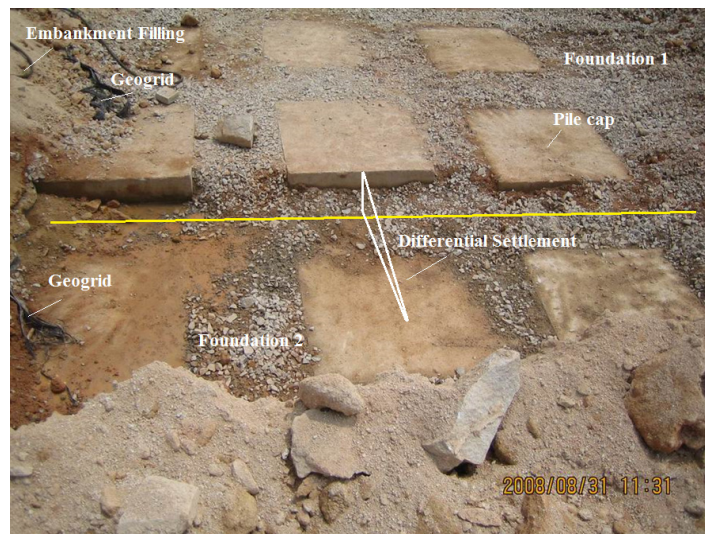


Fig. 2 Differential settlement of foundation

Table 2 Main reasons for embankment differential settlement of existing railways

Reason	Railways	Site Investigation
Regional land subsidence	Beijing-Shanghai Railway etc.	Yangcun: 30-35 mm/year; Yangliuqing: 40-50 mm/year; Jinghai: 30-40 mm/year. Obvious differential settlement.
Soft ground settlement	Hangzhou-Ningbo Railway etc.	When thickness of the soft soils is less than 6 m, post-construction settlement (15 years) of unreinforced foundation was 15.9 cm; When thickness of the soft soils was between 6-15 m, post-construction settlement of reinforced foundation was 6.7 cm. Differential settlement was 9.2 cm in the range of 100 m.
Different characteristics of embankment filler	Hangzhou-Ningbo Railway etc.	Ballast-pit depth was 80-90 cm with serious ponding
Embankment compactness differences	Zhejiang-Jiangxi Railway etc.	Differential settlement was 10-20 cm
Effect of dynamic loading	Shanghai-Hangzhou Railway etc.	Settlement rate of reinforced foundation and unreinforced foundation was 0.2 mm/day and 0.4 mm/day in construction separately, and in the first 30 days in operation, settlement rate of that was 0.3 mm/day and 0.44 mm/day.
Other nearby constructions	Beijing-Jiulong Railway etc.	Large embankment differential settlement was caused by box- culvert construction

obvious in the area of soft soils, expansive soils and collapsible loess where passenger and freight transportation is huge in China. The main reasons for embankment differential settlement of existing railways can be summarized as follows: (1) regional land subsidence; (2) soft ground settlement; (3) different characteristics of embankment filler; (4) embankment compactness differences; (5) effect of dynamic loading; and (6) other nearby constructions. It can draw a conclusion from the investigation of existing railways: controlling embankment post-construction settlement, especially differential settlement, is a key and difficult issue for embankment engineering in high-speed railways (Wang 2007, Shaer *et al.* 2008, Shin *et al.* 2002). Differential settlement has a significant impact on railway safe operation that had been already testified by our previous research work (Wang *et al.* 2013).

Embankment differential settlement generally exists in the area between different foundations, structures or ground treatments such as embankment-bridge transition section which has obvious different stiffness. In the last decade, technical measures to control embankment differential settlement were mainly concentrated in the following respects: (1) reinforced embankment itself; (2) change foundation treatment methods and parameters; (3) using new filling materials to reduce weight; (4) strict control of construction process and quality (Akira *et al.* 2003, Bergado and Teerawattanasuk 2008, Chen *et al.* 2008, Rowe and Li 2002, Abusharar *et al.* 2009, Han and Gabr 2002, Nakanishi and Takewaki 2013, Liu *et al.* 2007).

In conclusion, larger embankment differential settlement that may seriously endanger the safe

operation of railways can be caused by uneven characteristics of foundation. So far, general method for calculating embankment settlement which is based on total settlement controlling is used to control embankment settlement in the high-speed railways. That is cross-section calculation method which cannot fully reflect the characteristics and requirements for settlement controlling of high-speed railways. For this calculation method, embankment differential settlement which exists in the area between different foundations, structures or ground treatment cannot reasonably be computed. Furthermore, a lot of research work had been done on the settlement of horizontal layered foundation in the existing calculation theory. However, there is little research on the settlement of vertical bounding layer between different structures and foundations.

3. Centrifugal model test

3.1 Physical model

Vertical interface is an assumptive, theoretical and ideal vertical surface between foundations with different types of soils, structures and foundation treatment methods etc. The Mechanical behavior of such an interface between different materials has been paid more and more attention with using different foundation treatment methods and structure forms in high-speed railways. The simplified vertical interface of two materials is shown in Fig. 3.

3.2 Centrifugal test

Many factors, such as the properties of the foundation soil, the length and spacing of piles, gravel cushion (raft plate), affect the differential settlement of geogrid-reinforced pile-raft-supported embankments. This section mainly discusses the centrifugal test results of the differential settlement of geogrid-reinforced pile-raft-supported embankments, which is generally composed of subgrade, raft structure, gravel cushion, rigid pile and soil between piles, as shown in Fig. 4.

The centrifugal test model was made as 1:100 of the prototype, with the centrifugal acceleration of 100 g being used. The collapsible loess was obtained from the third level terrace of the Yellow River in Lanzhou, China. The soil properties in centrifugal model are given in Table 3. More details about the centrifugal tests can be found in Wang *et al.* (2013).

In the model test, the height of embankment was 6.0 m. The thickness of remolded collapsible loess layer was 15 m on top of a bearing stratum (2 m thick sand layer). The load of train and track

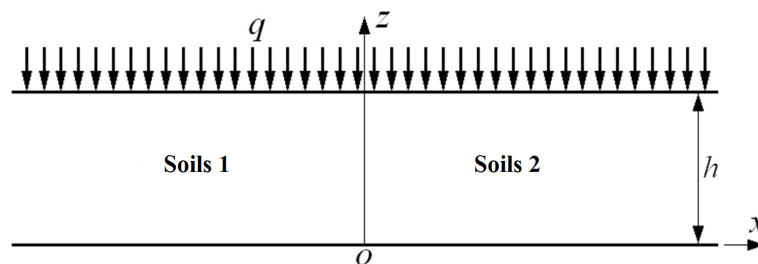


Fig. 3 The longitudinal section of the model of foundation

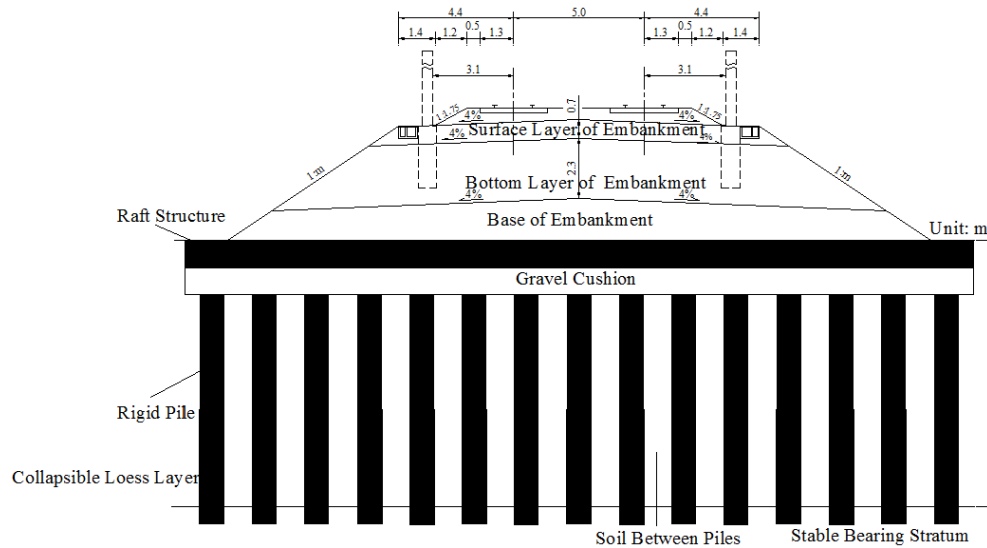


Fig. 4 Typical cross section of geogrid-reinforced pile-raft-supported embankments

Table 3 Index properties of soil in testing model

Soil	Density ρ (kg/m ³)	Water content ω (%)	Void ratio e	Saturation S_r (%)	Specific density G	Cohesion c (kPa)	Internal friction angle ϕ (°)
Collapsible loess	1600	19.0	1.02	50.7	2.71	16.6	24.3
Embankment filling	2080	19.0	0.55	93.5	2.71	35.1	30.3

Table 4 Summary of conditions and parameters of testing models

Type of tests	Thickness of embankment (m)	Thickness loess layer (m)	Load of train and track structure (m)	Pile spacing $D = 0.4$ m	Gravel cushion (cm)	Diameter of pile (m)	Reinforcedconcrete raft (cm)	Length of pile (m)	Diameter of particles (cm)
Centrifugal test	6.0	15.0	3.4 × 3.0	2D, 4D, 6D	30	0.4	45	16	2.5-4.0

structure was simulated by an equivalent soil column (3.4 m in width and 3.0 m in height, with the unit weight of 18.0 kN/m³). The pile spacing (s) was selected as $s = 2D, 4D$ and $6D$ with D being the pile diameter. A 30 cm thick gravel cushion with a layer of geogrid was constructed on top of the piles. In addition, polyester geogrid with the fiber spacing of 21.8 mm was placed in the middle height of the gravel cushion. For the raft structure, a 45 cm thick reinforced concrete slab was constructed on top of gravel cushion. The relevant material parameters are shown in Table 4. The configuration of the test model of geogrid-reinforced pile-raft-supported embankments,

including the arrangement of piles and the monitoring marks, is shown in Fig. 5. The simulation method of time in the centrifugal test was based on *Terzaghi's* one-dimensional consolidation theory (Taylor 1994).

3.3 Test results and analysis

Along the direction of a railway, the collapsible loess may be reinforced using piles with different spacing in various sections. As such differential settlement tends to take place between these sections. The differential settlements and differential settlement rates with different parameters of ground treatment (see Fig. 5) are shown in Fig. 6. In the construction stage, the total differential settlement between two sections with pile spacing of A_1 and A_2 was 3.14 cm ($A_1 = 4D$, $A_2 = 2D$), 13.71 cm ($A_1 = 6D$, $A_2 = 2D$) and 16.84 cm ($A_1 = 6D$, $A_2 = 2D$), respectively. The maximum differential settlement rate in these sections was 0.94 mm/day, 1.31 mm/day and 2.1 mm/day, respectively. In the post-construction stage, the total differential settlement with pile spacing of A_1 and A_2 was 1.77 cm ($A_1 = 4D$, $A_2 = 2D$), 1.29 cm ($A_1 = 6D$, $A_2 = 2D$) and 3.06 cm ($A_1 = 6D$, $A_2 = 2D$), correspondingly. The maximum differential settlement rate in these sections was 0.11 mm/day, 0.24 mm/day and 0.33 mm/day, respectively.

From experimental data, it observe that, with an increase of pile spacing (different reinforced foundations), the differential settlement and settlement rate increase especially in the construction stage. The differential settlement is also significantly affected by pile spacing in the post-construction stage.

Based on the test results mentioned above, in the following sections, we limit the discussion to the differential settlements on the two sides of the vertical interface of different reinforced foundations, while the mechanism of the geogrid-reinforced pile-raft-supported embankments to reduce settlement is not discussed. For simplicity, the geogrid-reinforced pile-raft-supported

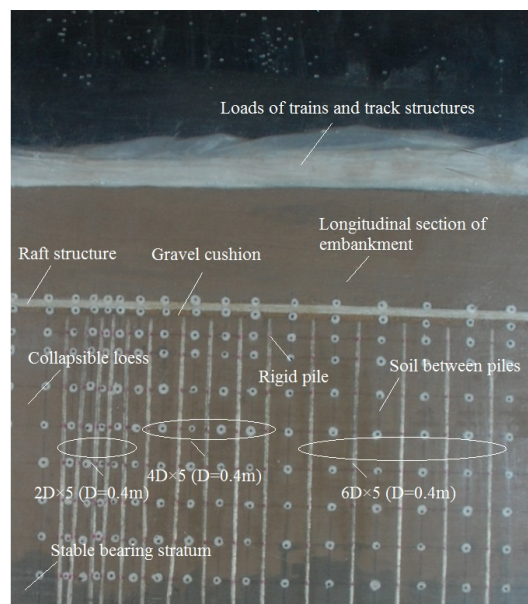
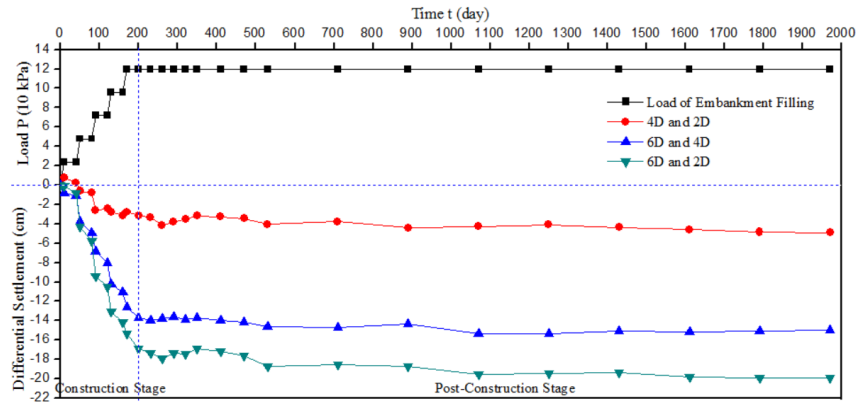
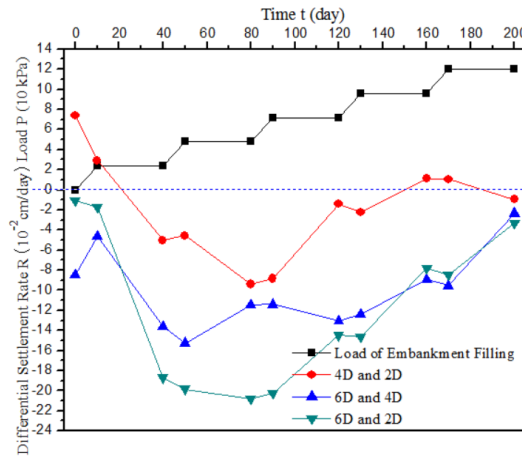


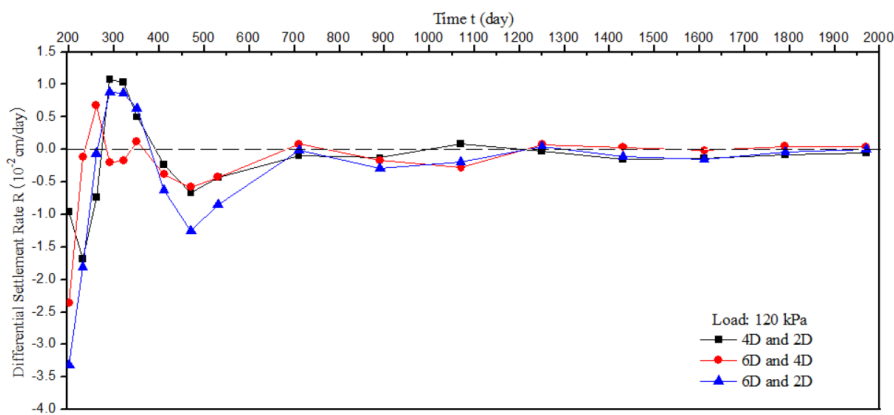
Fig. 5 Test model of geogrid-reinforced pile-raft-supported embankments



(a) Time dependent development of settlement



(b) Variation of settlement rate with time in construction stage

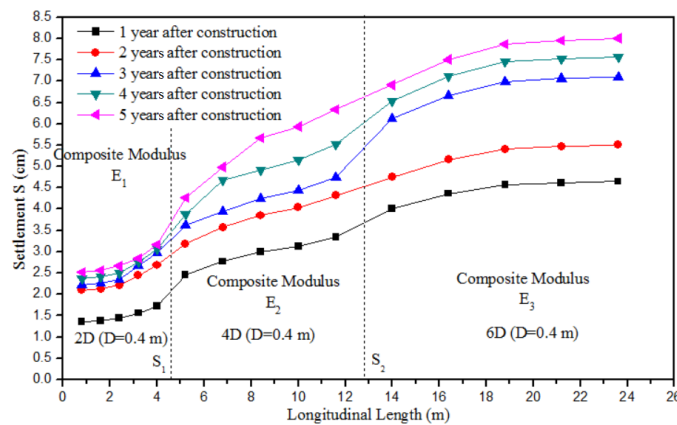


(c) Variation of settlement rate with time in post-construction stage

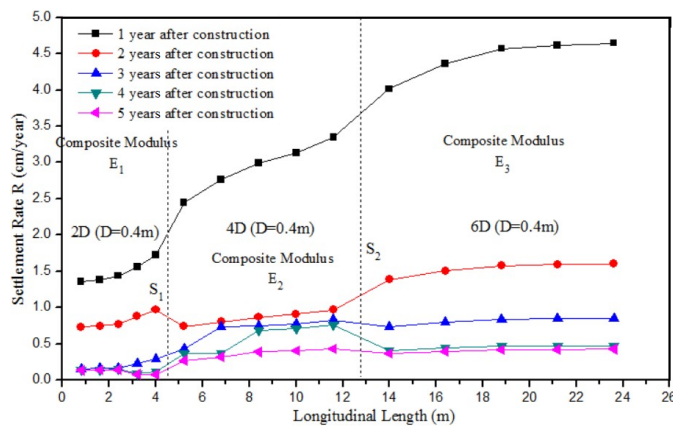
Fig. 6 Settlement of geogrid-reinforced pile-raft-supported embankments at different pile spacing: (a) time dependent development of settlement; (b) variation of settlement rate with time in construction stage; (c) variation of settlement rate with time in post-construction stage

embankments is simplified as a composite material having composite modulus E that is a function of soil's modulus E_s and pile modulus E_p and volume replacement rate n . The differential settlements and differential settlement rates on the two sides of the vertical interface between adjacent zones was treated as different pile structures (see Fig. 5) underneath the longitudinal central line of embankment, as shown in Fig. 7. The value of composite modulus E_1 , E_2 and E_3 was 71.9 MPa, 21.0 MPa and 11.5 MPa, respectively.

As can be seen from the Fig. 7, the longitudinal differential settlements and differential settlement rates exist obviously in the area of vertical interface S_1 which is the boundary of 2D zone (composite modulus is 71.9 MPa) with 4D zone (composite modulus is 21.0 MPa) and the boundary surface S_2 which is the boundary of 4D zone (composite modulus is 21.0 MPa) with 6D zone (composite modulus is 11.5 MPa). With an increase of time after construction under the same loading, the longitudinal differential settlements between different foundations increased. The differential settlement ratio also increased with time and gradually approached a relatively stable level. The average longitudinal differential settlements values on the two sides of S_1 and S_2 was



(a) Settlement



(b) Settlement rate

Fig. 7 Foundation settlement at different pile spacing with time in post-construction stage: (a) settlement; (b) settlement rate

1.44 cm and 1.51 cm, severally, at the end of 1st year after construction. Similarly, at the end of the 3rd year after construction, the average longitudinal differential settlement values on the two sides of S_1 and S_2 was 1.70 cm and 2.56 cm, and the average ratio of that was 0.22 cm/year and 1.13 cm/year, respectively. Finally, at the end of the 5th year after construction, the average longitudinal differential settlement value on the two sides of S_1 and S_2 was 2.69 cm and 2.21 cm, and the average ratio was 0.48 cm/year and -0.20 cm/year, respectively.

In summary, the centrifugal test results show that existing vertical interface can lead to obvious longitudinal differential settlement. The foundation that has lower modulus causes additional settlement (loading) more than that of larger modulus foundation. The attenuation rate of longitudinal settlement of larger modulus foundation changes much faster with time.

4. Establishment of analytical model

4.1 Basic assumptions

When establishing the analytical model, the following assumptions are made:

The length of embankment is infinite in longitudinal direction;

- (1) The influence depth of embankment is represented by h and there is no settlement in soils below this depth h (see Fig. 8). The properties of soils 1 and soils 2 on the two sides of the vertical interface are very different elastic materials;
- (2) The embankment load is a uniformly distributed load q , with the distribution width b_1 of embankment on the ground. On the cross section of embankment, the influence range of loading expands along a certain angle (the dotted lines shown in Fig. 9). The influence range of loading is b_0 at the depth of h below the ground.

For the simplicity of calculation, as shown in Fig. 9, the width of loading distribution at different depths is assumed to vary with the curves expressed as formula

$$b = b_0 e^{-kz/h} \quad (1)$$

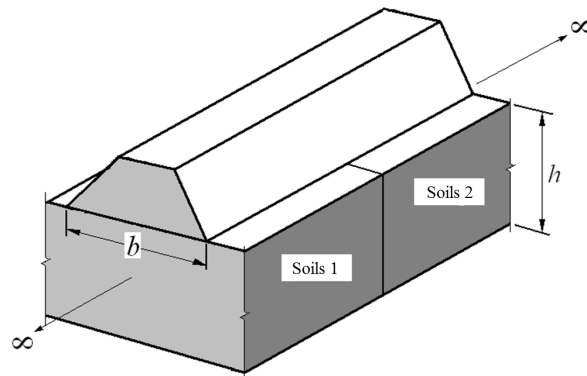


Fig. 8 The simplified model of embankment and foundation

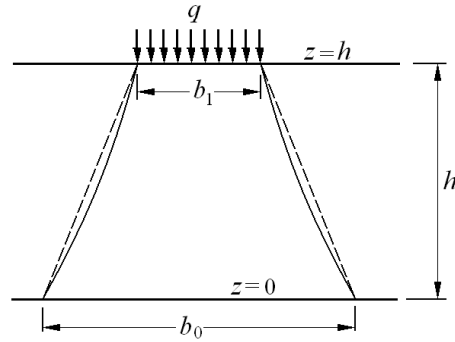


Fig. 9 The cross section of embankment model

Supposing the point $z = 0$ is the depth h below the ground, when $z = h$, $b = b_1$, $k = -\ln(b_1/b_0)$. The k is a graded coefficient, when $b_1 < b_0$, the k is positive. The cross section of embankment can be expressed as infinite strip of soils which is composed of two horizontal lines ($z = 0$, $z = h$) and two curves for researching. According to the equivalent section method, the infinite strip of soils is equivalent to a soil strip of fixed width (b_0) when the elastic modulus of the soil varies with depth according to the following expression

$$E = E_0 e^{-kz/h} \quad (2)$$

where E_0 is the elastic modulus at the point $z = 0$. The Poisson ratio ν of the materials is constant as $\nu = (\nu_1 + \nu_2)/2$, ν_1 for soil 1 and ν_2 for soil 2, respectively. Moreover, the plane strain condition is assumed for the analysis. In addition, we further assume

$$\frac{\rho_0^{(1)}}{E_0^{(1)}} = \frac{\rho_0^{(2)}}{E_0^{(2)}} = \frac{\rho_0}{E_0} = \text{Constant} \quad (3)$$

4.2 Basic equations

According to the elastic mechanics, the equilibrium equations of stresses are

$$\sigma_x = (\lambda + 2\mu) \frac{\partial u}{\partial x} + \lambda \frac{\partial w}{\partial z} \quad (4)$$

$$\sigma_z = (\lambda + 2\mu) \frac{\partial w}{\partial z} + \lambda \frac{\partial u}{\partial x} \quad (5)$$

$$\tau_{xz} = \mu \left(\frac{\partial w}{\partial x} + \frac{\partial u}{\partial z} \right) \quad (6)$$

where, σ_x , σ_z , σ_{xz} is normal stress in x and z direction and shear stress, respectively, u is the displacement in x direction, w is displacement in z direction. λ and μ are both material constants determined as

$$\lambda = \frac{Ev}{(1+\nu)(1-2\nu)} = \frac{\nu E_0 e^{-kz/h}}{(1+\nu)(1-2\nu)}, \quad \mu = \frac{E}{2(1+\nu)} = \frac{E_0 e^{-kz/h}}{2(1+\nu)} \quad (7)$$

Let us define

$$c = \frac{1}{2(1+\nu)}, \quad d = \frac{\nu}{(1+\nu)(1-2\nu)}, \quad a = d + 2c, \quad b = c + d \quad (8)$$

By inserting Eqs. (7) and (8) into Eqs. (2)-(5), we obtain

$$\frac{\partial \sigma_x}{\partial x} + \frac{\partial \tau_{xz}}{\partial z} = 0: \quad a \frac{\partial^2 u}{\partial x^2} + b \frac{\partial^2 w}{\partial x \partial z} - c \frac{k}{h} \frac{\partial w}{\partial x} - c \frac{k}{h} \frac{\partial u}{\partial z} + c \frac{\partial^2 u}{\partial z^2} = 0 \quad (9)$$

$$\frac{\partial \tau_{xz}}{\partial x} + \frac{\partial \sigma_z}{\partial z} - \rho g = 0: \quad c \frac{\partial^2 w}{\partial x^2} + b \frac{\partial^2 u}{\partial x \partial z} - a \frac{k}{h} \frac{\partial w}{\partial z} + a \frac{\partial^2 w}{\partial z^2} - d \frac{k}{h} \frac{\partial u}{\partial x} - \frac{\rho_0^{(j)}}{E_0^{(j)}} g = 0 \quad (10)$$

where ρ is soil density, ρ_0 is the soil density at point $z = 0$, and g is acceleration due to gravity. In Eq. (10), superscript $j = 1$ is on behalf of soils 1, and superscript $j = 2$ is on behalf of soils 2.

By taking into account the following boundary conditions

$$z = 0: \quad w = 0; \quad \tau_{xz} = 0$$

When $z = h$: $\sigma_z = -q$, when $x < 0, j = 1$; when $x > 0, j = 2$; $\tau_{xz} = 0$

The displacement function must satisfy

$$z = 0: \quad \frac{\partial w}{\partial x} + \frac{\partial u}{\partial z} = 0$$

$$z = h: \quad a \frac{\partial w}{\partial z} + d \frac{\partial u}{\partial x} = -\frac{q}{E_0^{(j)}}, \quad \text{where when } x < 0, j = 1; \quad \text{when } x > 0, j = 2; \quad \frac{\partial w}{\partial x} + \frac{\partial u}{\partial z} = 0$$

When $x \rightarrow \infty, u^{(1)} = 0$; ε_z and w should recover the strain and displacement values in a single material under the actions of self-weight and loading q in the form of

$$\begin{aligned} w^{(1)} &= -\frac{1}{aE_0^{(1)}} \int_0^z \left[\rho_0^{(1)} g \left(-\frac{h}{k} \right) \left(e^{-k+kz/h} - 1 \right) + q e^{kz/h} \right] \\ &= \frac{1}{a} \frac{\rho_0}{E_0} g \left(\frac{h}{k} \right) \left[\frac{h}{k} \left(e^{-k+kz/h} - e^{-k} \right) - z \right] - \frac{q}{aE_0^{(1)}} \left(\frac{h}{k} \right) \left(e^{kz/h} - 1 \right) \end{aligned} \quad (11)$$

4.3 Solution of equations

In order to find the solution of Eq. (10), we assume

$$w = \bar{w} + w^* \quad (12)$$

where

$$w^* = \frac{1}{a} \frac{\rho_0}{E_0} g \left(\frac{h}{k} \right) \left[\frac{h}{k} (e^{-k+ kz/h} - e^{-k}) - z \right] \tag{13}$$

When Eq. (13) is inserted in Eqs. (9) and (10), we have

$$a \frac{\partial^2 u}{\partial x^2} + b \frac{\partial^2 \bar{w}}{\partial x \partial z} - c \frac{k}{h} \frac{\partial \bar{w}}{\partial x} - c \frac{k}{h} \frac{\partial u}{\partial z} + c \frac{\partial^2 u}{\partial z^2} = 0 \tag{14}$$

$$c \frac{\partial^2 \bar{w}}{\partial x^2} + b \frac{\partial^2 u}{\partial x \partial z} - a \frac{k}{h} \frac{\partial \bar{w}}{\partial z} + a \frac{\partial^2 \bar{w}}{\partial z^2} - d \frac{k}{h} \frac{\partial u}{\partial x} = 0 \tag{15}$$

\bar{w} can be further decomposed into two parts

$$\bar{w} = \hat{w} + \tilde{w} \tag{16}$$

where

$$\tilde{w} = -\frac{q}{a} \left(\frac{h}{k} \right) (e^{kz/h} - 1) \left[\frac{1}{2E_0^{(1)}} (1 - \text{erf}(\xi)) + \frac{1}{2E_0^{(2)}} (1 + \text{erf}(\xi)) \right], \quad \xi = x/h \tag{17}$$

with $\text{erf}(\xi) = \frac{2}{\sqrt{\pi}} \int_0^\xi e^{-\xi^2} d\xi$ being the error function, and $\text{erf}(-\xi) = -\text{erf}(\xi)$, $\text{erf}(\infty) = 1$, $\text{erf}'(\xi) = \frac{2}{\sqrt{\pi}} e^{-\xi^2}$. As a result, Eqs. (14) and (15) become

$$\begin{aligned} & a \frac{\partial^2 u}{\partial x^2} + b \frac{\partial^2 \hat{w}}{\partial x \partial z} - c \frac{k}{h} \frac{\partial \hat{w}}{\partial x} - c \frac{k}{h} \frac{\partial u}{\partial z} + c \frac{\partial^2 u}{\partial z^2} \\ &= -b \frac{\partial^2 \tilde{w}}{\partial x \partial z} + c \frac{k}{h} \frac{\partial \tilde{w}}{\partial x} \\ &= \frac{q}{a} \left(-\frac{1}{2E_0^{(1)}} + \frac{1}{2E_0^{(2)}} \right) \left[b e^{kz/h} - c (e^{kz/h} - 1) \right] \frac{\text{erf}'(\xi)}{h} \end{aligned} \tag{18}$$

$$\begin{aligned} & c \frac{\partial^2 \hat{w}}{\partial x^2} + b \frac{\partial^2 u}{\partial x \partial z} - a \frac{k}{h} \frac{\partial \hat{w}}{\partial z} + a \frac{\partial^2 \hat{w}}{\partial z^2} - d \frac{k}{h} \frac{\partial u}{\partial x} \\ &= -c \frac{\partial^2 \tilde{w}}{\partial x^2} + a \frac{k}{h} \frac{\partial \tilde{w}}{\partial z} + a \frac{\partial^2 \tilde{w}}{\partial z^2} \\ &= \frac{qc}{a} \frac{k}{h} (e^{kz/h} - 1) \left(-\frac{1}{2E_0^{(1)}} + \frac{1}{2E_0^{(2)}} \right) \frac{\text{erf}''(\xi)}{h^2} \end{aligned} \tag{19}$$

where $\text{erf}'(\xi)$ and $\text{erf}''(\xi)$ is first- and second-order derivatives of $\text{erf}(\xi)$.

Using Eqs. (18) and (19) with the Fourier method, we obtain

$$-at^2U - bit \frac{\partial w}{\partial z} + c \frac{k}{h} itW - c \frac{k}{h} \frac{\partial U}{\partial z} + c \frac{\partial^2 U}{\partial z^2} = -P \left[b e^{kz/h} - c (e^{kz/h} - 1) \right] \text{Erf}'(t) \tag{20}$$

$$\begin{aligned}
& -ct^2U - bit \frac{\partial U}{\partial z} - a \frac{k}{h} \frac{\partial W}{\partial z} + a \frac{\partial^2 W}{\partial z^2} + d \frac{k}{h} itU \\
& = -Pc \frac{h}{k} (e^{kz/h} - 1) \text{Erf}''(t) = Pc \frac{h}{k} it (e^{kz/h} - 1) \text{Erf}'(t)
\end{aligned} \tag{21}$$

The general solutions of Eqs. (20) and (21) are

$$\bar{U} = A_1 e^{\alpha_1 tz} \cos \beta tz + A_2 e^{\alpha_1 tz} \sin \beta tz + A_3 e^{\alpha_2 tz} \cos \beta tz + A_4 e^{\alpha_2 tz} \sin \beta tz \tag{22}$$

$$\bar{W} = B_1 e^{\alpha_1 tz} \cos \beta tz + B_2 e^{\alpha_1 tz} \sin \beta tz + B_3 e^{\alpha_2 tz} \cos \beta tz + B_4 e^{\alpha_2 tz} \sin \beta tz \tag{23}$$

in which A_1 to A_4 are constant depending on the boundary conditions.

We set up the particular solutions of Eqs. (20) and (21) are $U^* = se^{kz/h} + l$, $W^* = me^{kz/h} + n$. The solutions of Eqs. (18) and (19) are

$$u = \frac{1}{\sqrt{2\pi}} \int_{-\infty}^{\infty} (A_1 e^{\alpha_1 tz} \cos \beta tz + A_2 e^{\alpha_1 tz} \sin \beta tz + A_3 e^{\alpha_2 tz} \cos \beta tz + A_4 e^{\alpha_2 tz} \sin \beta tz) e^{-ixt} dt \tag{24}$$

$$\begin{aligned}
\hat{w} = & \frac{1}{\sqrt{2\pi}} \int_{-\infty}^{\infty} \left(-ie^{\alpha_1 tz} [\cos \beta tz, \sin \beta tz] [G_1] \begin{Bmatrix} A_1 \\ A_2 \end{Bmatrix} - ie^{\alpha_2 tz} [\cos \beta tz, \sin \beta tz] [G_2] \begin{Bmatrix} A_3 \\ A_4 \end{Bmatrix} \right. \\
& \left. - i \frac{P}{t} \frac{h}{k} \text{Erf}'(t) (e^{kz/h} - 1) \right) e^{-ixt} dt
\end{aligned} \tag{25}$$

The constants A_1 to A_4 can be determined from the boundary conditions: When $z = 0$, $\hat{w} = 0$ we obtain $[1, 0] [G_1] \begin{Bmatrix} A_1 \\ A_2 \end{Bmatrix} + [1, 0] [G_2] \begin{Bmatrix} A_3 \\ A_4 \end{Bmatrix} = 0$

Sign $[G_1] = \begin{bmatrix} g_{11}^{(1)} & g_{12}^{(1)} \\ g_{21}^{(1)} & g_{22}^{(1)} \end{bmatrix}$, $[G_2] = \begin{bmatrix} g_{11}^{(2)} & g_{12}^{(2)} \\ g_{21}^{(2)} & g_{22}^{(2)} \end{bmatrix}$, it is found $g_{22}^{(1)} = g_{11}^{(1)}$, $g_{21}^{(1)} = -g_{12}^{(1)}$, $g_{22}^{(2)} = g_{11}^{(2)}$, $g_{21}^{(2)} = -g_{12}^{(2)}$.

So, it changes

$$g_{11}^{(1)} A_1 + g_{12}^{(1)} A_2 + g_{11}^{(2)} A_3 + g_{12}^{(2)} A_4 = 0 \tag{26}$$

When $z = 0$, $\frac{\partial \hat{w}}{\partial x} + \frac{\partial u}{\partial z} = 0$. We obtain

$$(\alpha_1 - g_{11}^{(1)}) A_1 + (\beta - g_{12}^{(1)}) A_2 + (\alpha_2 - g_{11}^{(2)}) A_3 + (\beta - g_{12}^{(2)}) A_4 = 0 \tag{27}$$

Using Eq. (26) it yields

$$\alpha_1 A_1 + \beta A_2 + \alpha_2 A_3 + \beta A_4 = 0 \tag{28}$$

When $z = h$, $\frac{\partial \hat{w}}{\partial x} + \frac{\partial u}{\partial z} = -P \left(\frac{h}{k} \right) (e^k - 1) \frac{\text{erf}'(\xi)}{h}$.

$$\begin{aligned}
 & e^{\alpha_1 ht} \left[(\alpha_1 - g_{11}^{(1)}) \cos(\beta ht) - (\beta - g_{12}^{(1)}) \sin(\beta ht), (\alpha_1 - g_{11}^{(1)}) \sin(\beta ht) + (\beta - g_{12}^{(1)}) \cos(\beta ht) \right] \begin{Bmatrix} A_1 \\ A_2 \end{Bmatrix} \\
 & e^{\alpha_2 ht} \left[(\alpha_2 - g_{11}^{(2)}) \cos(\beta ht) - (\beta - g_{12}^{(2)}) \sin(\beta ht), (\alpha_2 - g_{11}^{(2)}) \sin(\beta ht) + (\beta - g_{12}^{(2)}) \cos(\beta ht) \right] \begin{Bmatrix} A_3 \\ A_4 \end{Bmatrix} = 0
 \end{aligned} \tag{29}$$

When $z = h$

$$a \frac{\partial \hat{w}}{\partial z} + d \frac{\partial u}{\partial x} = -\frac{p}{E_0^{(j)}} e^k + p e^k \left[\frac{1}{2E_0^{(1)}} (1 - \operatorname{erf}(\xi)) + \frac{1}{2E_0^{(2)}} (1 + \operatorname{erf}(\xi)) \right] \tag{30}$$

when $x < 0, j = 1$; when $x < 0, j = 2$, then we obtain

$$\begin{aligned}
 & -i a t e^{\alpha_1 ht} \left[\alpha_1 \cos(\beta ht) - \beta \sin(\beta ht), \alpha_1 \sin(\beta ht) + \beta \cos(\beta ht) \right] \begin{Bmatrix} A_1 \\ A_2 \end{Bmatrix} \\
 & -i a t e^{\alpha_2 ht} \left[\alpha_2 \cos(\beta ht) - \beta \sin(\beta ht), \alpha_2 \sin(\beta ht) + \beta \cos(\beta ht) \right] \begin{Bmatrix} A_3 \\ A_4 \end{Bmatrix} \\
 & -i a t e^{\alpha_1 ht} \left[\cos(\beta ht), \sin(\beta ht) \right] \begin{Bmatrix} A_1 \\ A_2 \end{Bmatrix} - i a t e^{\alpha_2 ht} \left[\cos(\beta ht), \sin(\beta ht) \right] \begin{Bmatrix} A_3 \\ A_4 \end{Bmatrix} - i \frac{Pa}{t} e^k \operatorname{Erf}'(t) \\
 & = -\frac{1}{\sqrt{2\pi}} \int_{-\infty}^{\infty} P a e^k (1 + \operatorname{erf}(\xi)) e^{itx} dx + \frac{1}{\sqrt{2\pi}} \int_{-\infty}^{\infty} P a e^k (1 - \operatorname{erf}(\xi)) e^{itx} dx
 \end{aligned} \tag{31}$$

where, the first item on the right-hand side is

$$\begin{aligned}
 & -\frac{1}{\sqrt{2\pi}} \int_{-\infty}^{\infty} P a e^k (1 + \operatorname{erf}(\xi)) e^{itx} dx \\
 & = -\frac{1}{\sqrt{2\pi}} \int_{-\infty}^{\infty} P a e^k (1 + \operatorname{erf}(\xi)) e^{it(-x)} d(-x) = -\frac{1}{\sqrt{2\pi}} \int_0^{\infty} P a e^k (1 - \operatorname{erf}(\xi)) e^{-itx} dx
 \end{aligned} \tag{32}$$

After inserting Eq. (32), Eq. (31) on the right-hand side changes to

$$\begin{aligned}
 & -\frac{1}{\sqrt{2\pi}} \int_0^{\infty} P a e^k (1 - \operatorname{erf}(\xi)) e^{-itx} dx + \frac{1}{\sqrt{2\pi}} \int_0^{\infty} P a e^k (1 - \operatorname{erf}(\xi)) e^{itx} dx \\
 & = i \sqrt{\frac{2}{\pi}} \int_0^{\infty} P a e^k \operatorname{erfc}(\xi) \sin x t dx
 \end{aligned} \tag{33}$$

where, $\operatorname{erfc}(\xi)$ is the complementary error function.

Eq. (29) can be rewritten as

$$\begin{aligned}
 & -e^{\alpha_1 ht} \left[\alpha_1 \cos(\beta ht) - \beta \sin(\beta ht), \alpha_1 \sin(\beta ht) + \beta \cos(\beta ht) \right] \begin{Bmatrix} A_1 \\ A_2 \end{Bmatrix} \\
 & -e^{\alpha_2 ht} \left[\alpha_2 \cos(\beta ht) - \beta \sin(\beta ht), \alpha_2 \sin(\beta ht) + \beta \cos(\beta ht) \right] \begin{Bmatrix} A_3 \\ A_4 \end{Bmatrix}
 \end{aligned} \tag{34}$$

↓

$$\begin{aligned}
 & \uparrow \\
 & -\frac{d}{a} e^{\alpha_1 ht} [\cos(\beta ht), \sin(\beta ht)] \begin{Bmatrix} A_1 \\ A_2 \end{Bmatrix} - \frac{d}{a} e^{\alpha_2 ht} [\cos(\beta ht), \sin(\beta ht)] \begin{Bmatrix} A_3 \\ A_4 \end{Bmatrix} \quad (34) \\
 & = \sqrt{\frac{2}{\pi}} \frac{P}{t^2} e^k
 \end{aligned}$$

The constants A_1, A_2, A_3, A_4 can be obtained by solving the linear equation system of Eqs. (25), (26), (27) and (29).

Finally, using Eqs. (12), (13), (14), (15) and (25), we obtain the expression of vertical settlement

$$\begin{aligned}
 w = & \sqrt{\frac{2}{\pi}} \int_0^\infty \left(-e^{\alpha_1 tz} [\cos(\beta tz), \sin(\beta tz)] \begin{Bmatrix} A_1 \\ A_2 \end{Bmatrix} - ie^{\alpha_2 tz} [\cos(\beta tz), \sin(\beta tz)] \begin{Bmatrix} A_3 \\ A_4 \end{Bmatrix} \right) \sin(xt) dt \\
 & - \frac{P}{t} \frac{2}{\pi} \int_0^\infty \frac{e^{-t^2 h^2 / 4}}{t} (e^{kz/h} - 1) \sin(xt) dt - \frac{q}{a} \left(\frac{h}{k} \right) (e^{kz/h} - 1) \left[\frac{1}{2E_0^{(1)}} (1 - \operatorname{erf}(\xi)) + \frac{1}{2E_0^{(2)}} (1 + \operatorname{erf}(\xi)) \right] \quad (35) \\
 & + \frac{1}{a} \frac{\rho_0}{E_0} g \left(\frac{h}{k} \right) \left[\frac{h}{k} (e^{-k+kz/h} - e^{-k}) - z \right]
 \end{aligned}$$

The horizontal displacement can be readily calculated using Eq. (24).

5. Result analysis, comparison and evaluation

5.1 Case 1: theoretical values at various depths in one model

The following parameters are used in this example: equivalent elasticity modulus $E_0^{(1)}$ is 220 MPa and equivalent density $\rho_0^{(1)}$ is 2400 kg/m³ of embankment soils 1, and equivalent elasticity modulus $E_0^{(2)}$ is 100 MPa and equivalent density $\rho_0^{(2)}$ is 2000 kg/m³ of embankment soils 2. (when $z = h$ in Eq. (1), actual elastic modulus $E_0^{(1)}$ is 115.3 MPa and actual density $\rho_0^{(1)}$ is 1257.2 kg/m³ of embankment soils 1, and actual elastic modulus $E_0^{(2)}$ is 52.4 MPa and actual density $\rho_0^{(2)}$ is 1047.7 kg/m³ of embankment soils 2). The average value of the Poisson ratio ν is 0.35 and distributed load q is 80 kPa. Influencing depth of load is 10 m with embankment distribution width $b_1 = 11$ m, $b_0 = 21$ m. Summary of calculation parameters of theoretical model is shown in Table 5. The calculation results are shown in Fig. 10.

The calculation results show that integral convergence of infinite field is quick in theory, and upper limit is from 20 to 30 m. The distribution of settlement on both sides of vertical interface of different soils is very reasonable. The differential settlement on both sides of vertical interface decreases with the increase of depth. The settlement tends to become stable at about 20 m away from the vertical interface.

5.2 Case 2: theoretical values at surface layer in various models

The Calculation parameters (as summarized in Table 5) are used in this example: equivalent

Table 5 Summary of calculation parameters of theoretical model in 3 cases

	Poisson ratio ν	Load q (kPa)	b_1 (m)	b_0 (m)	Soil 1		Soil 2		
					Elasticity modulus $E_0^{(1)}$ (MPa)	Density $\rho_0^{(1)}$ (kg/m ³)	Elasticity modulus $E_0^{(2)}$ (MPa)	Density $\rho_0^{(2)}$ (kg/m ³)	
Case 1	0.35	80	11	21	220	2400	100	2000	
Case 2	0.32	60	11	21	120	2400	S_1	180	2600
							S_2	220	2800
							S_3	260	3000
							S_4	300	3200
Case 3	0.419	141.3	13.8	21.8	71.9	1937	2D-4D	21.0	1834.4
	0.434				21.0	1834.4	4D-6D	11.5	1815.3

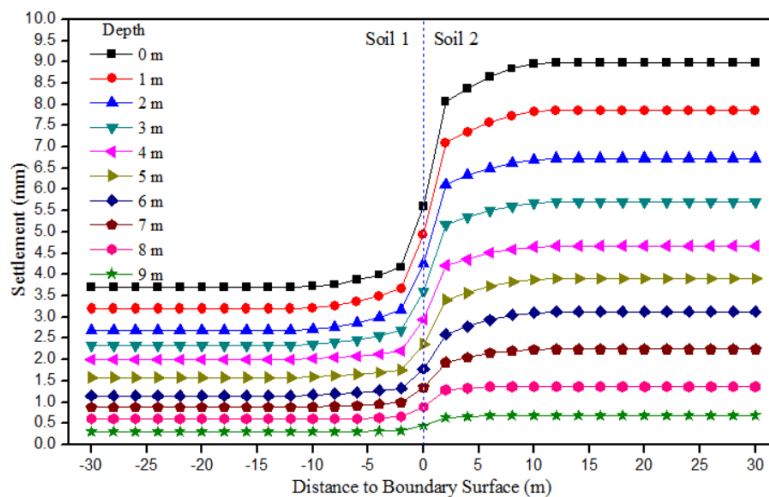


Fig. 10 Theoretical values of settlements at various depths in one model

elasticity modulus $E_0^{(1)}$ is 120 MPa and equivalent density $\rho_0^{(1)}$ is 2400 kg/m³ of embankment soils 1. Four parameter of groups of embankment soils 2: S_1 , equivalent elastic modulus $E_0^{(1)}$ is 180 MPa and equivalent density $\rho_0^{(1)}$ is 2600 kg/m³; S_2 , equivalent elastic modulus $E_0^{(1)}$ is 220 MPa and equivalent density $\rho_0^{(1)}$ is 2800 kg/m³; S_3 , equivalent elastic modulus $E_0^{(1)}$ is 260 MPa and equivalent density $\rho_0^{(1)}$ is 3000 kg/m³; And S_4 , equivalent elastic modulus $E_0^{(1)}$ is 300 MPa and equivalent density $\rho_0^{(1)}$ is 3200 kg/m³. In all calculation models, The average value of Poisson ratio ν is 0.32 and load q is 60 kPa. Influencing depth of load is 10 m with embankment distribution width $b_1 = 11$ m, $b_0 = 21$ m. It can see the calculation results from Fig. 11.

With the increase of elastic modulus of embankment soils 2, the differential settlements of two sides of the vertical interface increase significantly and it becomes larger slightly for the scope of the settlement. The differences between moduli of soils are the primary cause of the differential settlements.

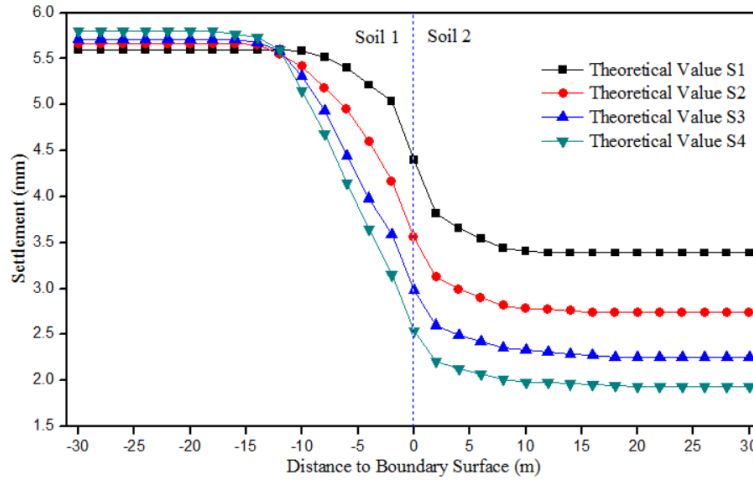


Fig. 11 Theoretical values of settlements at surface layer in various models

5.3 Case 3: comparative analysis on theoretical values and test values

Calculating parameters (as shown in Table 5): equivalent elasticity modulus E_1 is 71.9 MPa and equivalent density ρ_1 is 1937 kg/m³ of 2D piled composite foundation, and equivalent elasticity modulus E_2 is 21.0 MPa and equivalent density ρ_2 is 1834.4 kg/m³ of 4D piled composite foundation, and equivalent elasticity modulus E_3 is 11.5 MPa and equivalent density ρ_3 is 1815.3 kg/m³ of 6D piled composite foundation. Influencing depth of load is 30 m with embankment distribution width $b_1 = 13.8$ m, $b_0 = 21.8$ m. The Poisson ratio of 2D-4D piled composite foundation is 0.419 and the Poisson ratio of 4D-6D piled composite foundation is 0.434. Load q is 141.3 kPa.

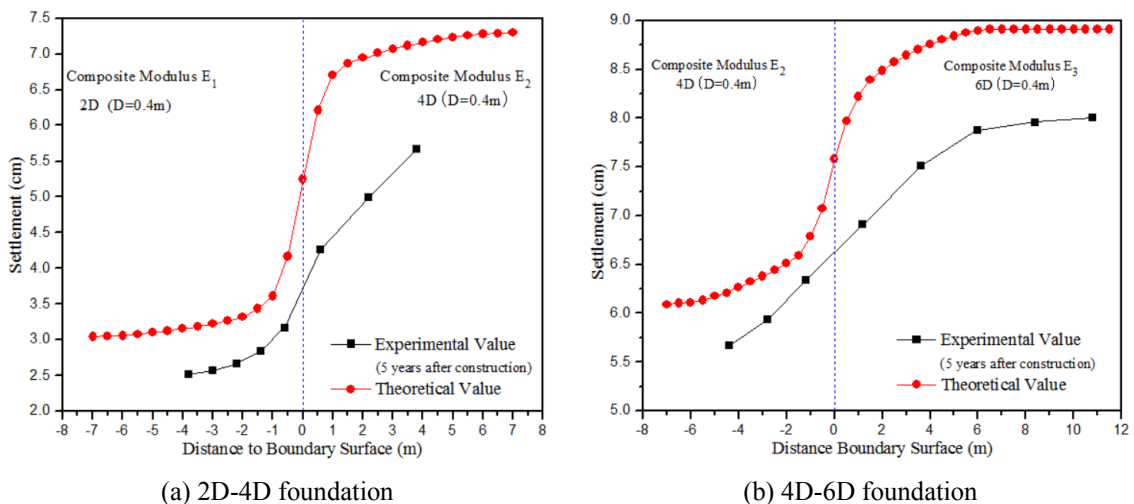


Fig. 12 Comparative analysis on theoretical values and experimental values: (a) 2D-4D foundation; (b) 4D-6D foundation

Fig. 12 qualitatively compares the differential settlement on both sides of a vertical interface between different material zones, as obtained from the theoretical analysis and centrifugal model tests. We observe that the analytical model correctly captures the general trend of differential settlement variation as compared with the test results. The difference between the theoretical and experimental results is small on the side of soils with smaller modulus, but significant error is observed on the side of soils with larger modulus. Under the same loading conditions, the settlement of the foundation with larger modulus of deformation (or elastic modulus) is less. Therefore, the ratio of increment value and settlement value (theoretical values or test values) is larger, that is, attenuation rate is more significant (or change much faster).

Regarding the significant errors of differential settlement on the side of soils with larger modulus as illustrated in Fig. 12, there are four major reasons:

- (1) Differences in applied load: In the theoretical model, the embankment is assumed as an infinite strip of soils in longitudinal direction. However, this is unachievable in the model tests, in which the Embankment load was simulated by limited length of uniformly distributed load.
- (2) Differences in foundation (soils) characteristics: In the theoretical model, the foundations (soils) are assumed to be homogeneous, elastic and isotropic in the infinite half space. However, not all of these assumptions are satisfied in the model tests.
- (3) Modulus conversion: The compression modulus or the deformation modulus can be easily obtained from geotechnical tests, while the determination of elastic modulus is not a trivial task in the theoretical calculation. In addition, the assumption about the variation of elastic modulus with depth in the analytical model may be different from the actual soil behaviour.
- (4) The effect of soil internal friction. Effect of soil internal friction is significant, in particular with fine sands, which can make a vital impact on additional stress transmission and diffusion, as well as settlement.

6. Conclusions

The following conclusions can be drawn from this research:

- The railway operation state deterioration phenomenon caused by embankment differential settlement is widespread in soft soils especially in the area between different foundations or structures. The main reasons for embankment differential settlement can be summarized as follows: (a) regional land subsidence; (b) soft ground settlement; (c) uneven characteristics of embankment filler; (d) embankment compactness differences; (e) effect of dynamic loading; (f) other nearby constructions.
- Both in horizontal and vertical directions, evident differential settlement exists on both sides of the vertical interface, which is a limited area between different foundations. The foundation which has larger elastic modulus can undertake and transfer more additional stress and cause relatively less settlement. Differential settlement value decreases as the distance to vertical interface decreases. With the relative modulus value of different foundations increasing, foundation settlement which has lower elastic modulus gets larger settlement. Meanwhile, differential settlement is more obvious.
- The calculation results show that integral convergence of infinite field is quick in theory, and upper limit is from 20 to 30 m. The distribution of settlement which is on both sides of

the vertical interface of different soils is very reasonable. The differential settlement which exists observably on both sides of the vertical interface reduces with the increasing of depth. Settlement tends to be stable about 20 m from the vertical interface. The differences of modulus are the main reason of causing material (soils) stiffness differences, and also is the primary cause of differential settlements.

- The significant errors of differential settlement between theoretical values and test values exist in both sides of soils. There are four major reasons: (a) different load form; (b) foundation characteristics differences; (c) modulus conversion; (d) effect of soil internal friction

Acknowledgments

This research is financially supported by the National High Technology Research and Development Program of China (Grant No. 2007AA11Z116).

References

- Abusharar, S.W., Zheng, J.J., Chen, B.G. and Yin, J.H. (2009), "A simplified method for analysis of a piled embankment reinforced with geosynthetics", *Geotext. Geomembr.*, **27**(1), 39-52.
- Akira, S., Lawalenna, S. and Norihiko, M. (2003), "Partially-drained cyclic behavior and its application to the settlement of a low embankment road on silty-clay", *Soil. Found.*, **43**(1), 33-46.
- Anderson, J., Townsend, F. and Rahelison, L. (2007), "Load testing and settlement prediction of shallow foundation", *J. Geotech. Geoenviron.*, **133**(12), 1494-1502.
- Bergado, D.T. and Teerawattanasuk, C. (2008), "2D and 3D numerical simulations of reinforced embankments on soft ground", *Geotext. Geomembr.*, **26**(1), 39-55.
- Braja, M.D. (2008), *Advanced Soil Mechanics*, (3rd Edition), Taylor & Francis, New York, NY, USA.
- Chen, Y.M., Cao, W.P., and Chen, R.P. (2008), "An experimental investigation of soil arching within basal reinforced and unreinforced piled embankments", *Geotext. Geomembranes.*, **26**(2), 164-174.
- Fenton, G. and Griffiths, D. (2002), "Probabilistic foundation settlement on spatially random soil", *J. Geotech. Geoenviron.*, **128**(5), 381-390.
- Han, J. and Gabr, M. (2002), "Numerical analysis of geosynthetic-reinforced and pile-supported earth platforms over soft soil", *J. Geotech. Geoenviron.*, **128**(1), 44-53.
- Liu, H.L., Charles, W.W. and Fei, K. (2007) "Performance of a geogrid-reinforced and pile-supported highway embankment over soft clay: Case study", *J. Geotech. Geoenviron.*, **133**(12), 1483-1493.
- Matyas, E.L. and Rothenburg, L. (1996), "Estimation of total settlement of embankments by field measurements", *Can. Geotech. J.*, **33**(5), 834-841.
- Ministry of Railways of People's Republic of China (2009), Code For Design Of High Speed Railway (TB10621-2009), Beijing, China.
- Mutsumi, T., Toshihiro, N., Motohiro, I., Masaki, N. and Akira, A. (2011), "Prediction of settlement in natural deposited clay ground with risk of large residual settlement due to embankment loading", *Soil. Found.*, **51**(1), 133-149.
- Mylonakis, G. and Gazetas, G. (1998), "Settlement and additional internal forces of grouped piles in layered soil", *Géotechnique*, **48**(1), 55-72.
- Nakanishi, K. and Takewaki, L. (2013), "Optimum pile arrangement in piled raft foundation by using simplified settlement analysis and adaptive step-length algorithm", *Geomech. Eng., Int. J.*, **5**(6), 519-540.
- Puzrin, A.M., Alonso, E.E. and Pinyo, N.M. (2010), *Geomechanics of Failures*, Springer, Heidelberg, Germany.
- Rowe, R.K. and Li, L.A. (2002), "Behaviour of reinforced embankments on soft rate-sensitive soils",

- Géotechnique*, **52**(1), 29-40.
- Shaer, A.A., Duhamel, D., Sab, K., Foret, G. and Schmitt, L. (2008), "Experimental settlement and dynamic behavior of a portion of ballasted railway track under high speed trains", *J. Sound. Vib.*, **316**(1-5), 211-233.
- Shin, E.C., Kim, D.H. and Das, B.M. (2002), "Geogrid-reinforced railroad bed settlement due to cyclic load", *Geotech. Geol. Eng.*, **20**(3), 261-271.
- Shideh, D., Jonathan, D.B., Juan, M.P., Michael, R. and Dan, W. (2010), "Mechanisms of seismically induced settlement of buildings with shallow foundations on liquefiable soil", *J. Geotech. Geoenviron.*, **136**(1), 151-164.
- Taylor, R.N. (1994), *Geotechnical Centrifuge Technology*, CRC Press, Boca Raton, FL, USA.
- Toshihiro, N., Akira, A., Masaki, N., Eiji, Y. and Mutsumi, T. (2005), "Progressive consolidation settlement of naturally deposited clayey soil under embankment loading", *Soils. Found.*, **45**(5), 39-51.
- Wang, B.L. (2007), *Embankment Engineering in High-Speed Railways*, China Railway Press, Beijing, China.
- Wang, C.D., Wang, B.L., Guo, P.J. and Zhou, S.H. (2013), "Experimental analysis on settlement controlling of geogrid-reinforced pile-raft-supported embankments in high-speed railway", *Acta. Geotech.*, DOI: 10.1007/s11440-013-0288-6
- Wang, C.D., Zhou, S.H., Guo, P.J. and Wang, B.L. (2014), "Experimental analysis on settlement controlling of geogrid-reinforced pile-supported embankments on collapsible loess in high-speed railway", *Int. J. Pavement. Eng.*, **15**(9), 867-878.
- Wang, Z.L., Li, Y.C. and Shen, R.F. (2007), "Correction of soil parameters in calculation of embankment settlement using a BP network back-analysis model", *Eng. Geol.*, **91**(2-4), 168-177.
- Wu, W. and Yu, H.S. (2006), *Modern Trends in Geomechanics*, Springer, Heidelberg, Germany.